Human Molecular Genetics, 2015, Vol. 24, No. 9 2482–2491

doi: 10.1093/hmg/ddv009
Advance Access Publication Date: 18 January 2015
Original Article

ORIGINAL ARTICLE

A missense mutation in DCDC2 causes human recessive deafness *DFNB66*, likely by interfering with sensory hair cell and supporting cell cilia length regulation

M'hamed Grati[1,†], Imen Chakchouk[2,†], Qi Ma[1,‡], Mariem Bensaid[2,‡], Alexandra Desmidt[3,‡], Nouha Turki[4], Denise Yan[1], Aissette Baanannou[2], Rahul Mittal[1], Nabil Driss[4], Susan Blanton[5], Amjad Farooq[6], Zhongmin Lu[3], Xue Zhong Liu[1,*] and Saber Masmoudi[2,*]

[1]Department of Otolaryngology, University of Miami Miller School of Medicine, Miami, FL 33136, USA, [2]Laboratoire Procédés de Criblage Moléculaire et Cellulaire, Centre de Biotechnologie de Sfax, Université de Sfax, Sfax, Tunisie, [3]Department of Biology, University of Miami, Miami, FL 33146, USA, [4]Service Otorhinolaryngologie, Hôpital Universitaire Mahdia, Mahdia, Tunisie, [5]Dr John T. Macdonald Foundation Department of Human Genetics, and John P. Hussman Institute for Human Genomics, University of Miami, Miami, FL 33146, USA and [6]Biochemistry and Molecular Biology, University of Miami Miller School of Medicine, Miami, FL 33136, USA

*To whom correspondence should be addressed at: Department of Otolaryngology (D-48), University of Miami, 1666 NW 12th Avenue, Miami, FL 33136, USA. Tel: +1 3052431484; Fax: +1 3052432009; Email: xliu@med.miami.edu (X.Z.L.); Laboratoire Procédés de Criblage Moléculaire et Cellulaire, Centre de Biotechnologie de Sfax. Route sidimansour Km 6, BP '1177', 3018 Sfax, Tunisie. Tel: +216 98667620; Fax: +216 74875818; Email: saber.masmoudi@cbs.rnrt.tn (S.M.)

Abstract

Hearing loss is the most common sensory deficit in humans. We show that a point mutation in DCDC2 (DCDC2a), a member of doublecortin domain-containing protein superfamily, causes non-syndromic recessive deafness *DFNB66* in a Tunisian family. Using immunofluorescence on rat inner ear neuroepithelia, DCDC2a was found to localize to the kinocilia of sensory hair cells and the primary cilia of nonsensory supporting cells. DCDC2a fluorescence is distributed along the length of the kinocilium with increased density toward the tip. DCDC2a-GFP overexpression in non-polarized COS7 cells induces the formation of long microtubule-based cytosolic cables suggesting a role in microtubule formation and stabilization. Deafness mutant DCDC2a expression in hair cells and supporting cells causes cilium structural defects, such as cilium branching, and up to a 3-fold increase in length ratios. In zebrafish, the ortholog *dcdc2b* was found to be essential for hair cell development, survival and function. Our results reveal *DCDC2a* to be a deafness gene and a player in hair cell kinocilia and supporting cell primary cilia length regulation likely via its role in microtubule formation and stabilization.

Introduction

The high prevalence/incidence of hearing impairment in man makes it the most common sensory defect. It affects one in nearly 500 newborns and the majority of cases are of genetic origin. Hereditary hearing loss (HL) that is associated with no other symptoms, classified as non-syndromic deafness, is extremely

† M.G. and I.C. contributed equally to this study.
‡ Q.M., M.B. and A.D. contributed equally to this study.

Received: November 4, 2014. **Revised:** January 8, 2015. **Accepted:** January 13, 2015

heterogeneous. Non-syndromic genetic hearing loss is inherited in an autosomal recessive mode (ARNSHL) in ~77% of the cases, autosomal dominant HL (ADNSHL) accounts for about 22%, and the remaining ~1% is composed of X-linked and mitochondrial forms. Over 100 ARNSHL gene loci have been localized through genome-wide linkage analysis of large pedigrees of consanguineous families, and over 60 ARNSHL genes have been so far identified by positional cloning (http://hereditaryhearingloss.org/). Many of the identified proteins play key roles in hair cell mechanosensory stereocilia hair bundle development via its positioning and orientation, in its maturation via stereocilia length and thickness regulation and hair bundle cohesion, and in the molecular makeup and operation of hair cell mechanotransduction machinery (reviewed in 1).

We have mapped a 16.5-Mb critical region, which segregated in a large consanguineous Tunisian family, FT2, associated with autosomal recessive non-syndromic hearing impairment (ARNSHI) (*DFNB66*), to human chromosome 6p21.2–22.3 (2) (Fig. 1A). Using Sanger sequencing, we excluded *COL11A2*, *BAK1* and *LHFLP5* (also known as *TMHS*) in *DFNB66* (2,3). Here, using whole exome sequencing, we identified *DCDC2* (*DCDC2a*) as the causative gene for *DFNB66*. We localized DCDC2a to hair cell and supporting cells microtubule-based cilia and we demonstrate its potential key role in regulating microtubule nucleation, stability and length, and overall role in hair cell development and viability.

Results

Using whole exome sequencing, we identified a homozygous mutation (c.1271A>C, p.Gln424Pro; Fig. 1B) in a highly conserved residue (Fig. 1C) of *DCDC2* (*DCDC2a*; NM_001195610) that cosegregated with profound congenital deafness (Fig. 1E), that presented a loss of >70 dB for all tested frequencies. *DCDC2a* lies distal to

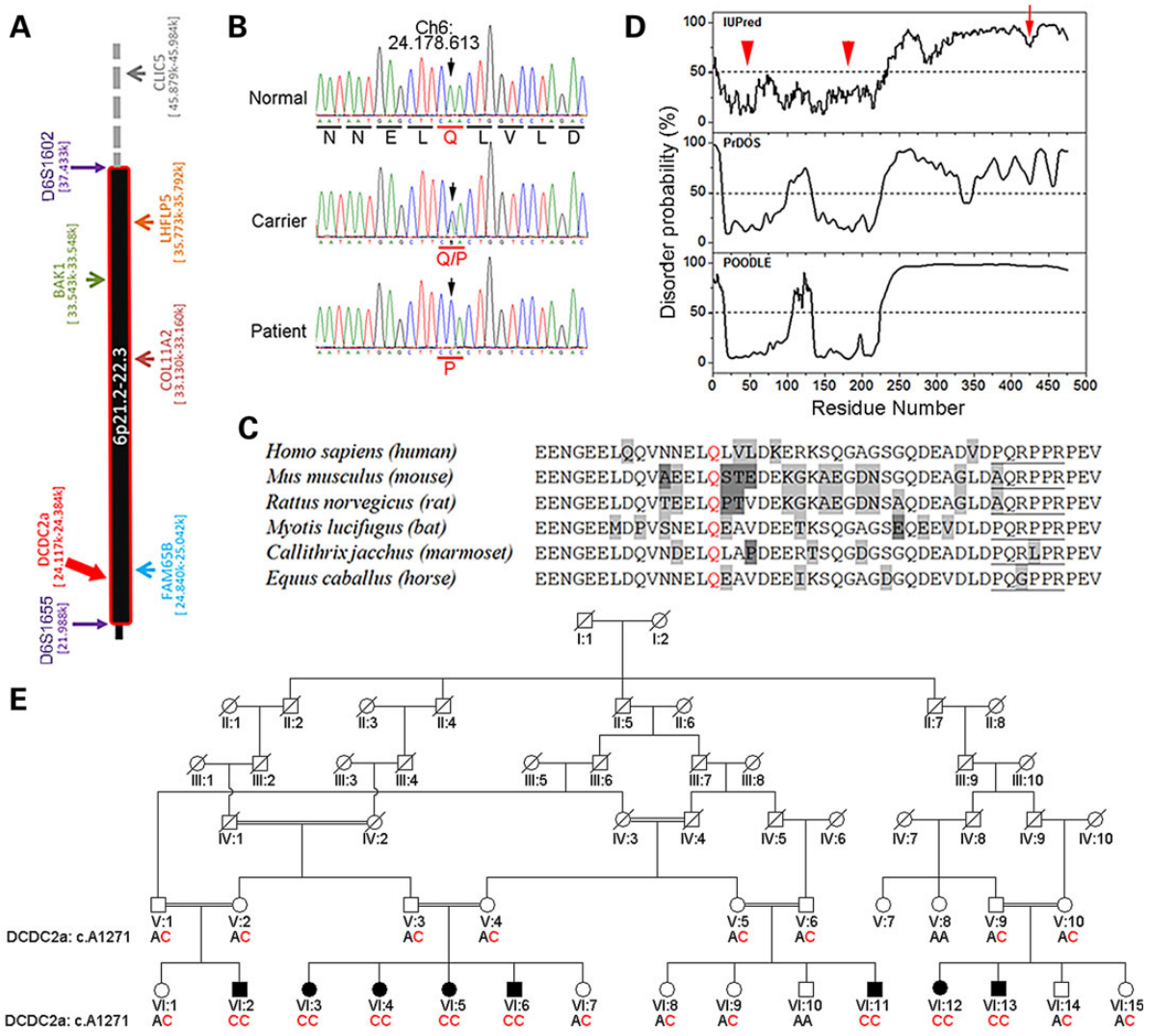

Figure 1. Molecular genetic and structural analysis of DCDC2a mutation. (**A**) DFNB66 locus on chromosome 6p21.2–22.3 pinpointing to the location of several known deafness genes and DCDC2a within the interval of interest. (**B**) Electrofluorograms of normal individual (VI:10), heterozygous individual (VI:7) and patient (VI:3) showing the identification of c.1271A>C nucleic substitution (ch6:24178613) causing p.Gln424Pro amino acid substitution in FT2 family. (**C**) Interspecies alignment of DCDC2a amino acid sequences around residue p.Gln424 (red) showing its high conservation. Underlined amino acid sequence corresponds to a predicted SH3-domain protein-binding motif, highly conserved among the different species. (**D**) Structural disorder probability plots of the full-length human DCDC2a, using IUPred, PrDOS and Poodle prediction software showing its two highly organized N-terminal doublecortin domains (arrowheads), and the highly unstructured C-terminal tail where DCDC2a mutation was found (Arrow). (**E**) Family FT2 pedigree with all genotyped individuals for DCDC2a c.A1271 alleles.

FAM65B (Fig. 1A), a gene that we recently identified as causing a form of ARNSHI in a Turkish family (4). Examination of the nucleic acid variants as well as exon copy number variants in *FAM65B* has excluded it from being the cause of deafness in FT2. Three additional homozygous variants corresponding to rs11752608 in *OR12D2*, rs117160266 in *FKBPL*, rs202138789 in *EGFL8* did not cosegregate with deafness within the family and were therefore excluded from being disease-causing. We did not identify the c.1271A>C mutation in 435 ancestry-matched healthy individuals, among the 6503 individuals listed in the National Heart, Lung and Blood Institute (NHLBI) Exome Sequencing Project variant database (EVS; http://evs.gs.washington.edu/EVS/), in dbSNP (http://www.ncbi.nlm.nih.gov/projects/SNP/), nor in the 1000 Genome Project database (http://browser.1000genomes.org/index.html). Polyphen-2 (score = 0.994; http://genetics.bwh.harvard.edu/pph2/), SIFT (score = 0.004; http://sift.bii.a-star.edu.sg/www/SIFT_related_seqs_submit.html) and MutationTaster (score = 0.76; http://mutationtaster.org/) predicted the p.Gln424Pro DCDC2a mutation to be deleterious.

In order to understand the molecular basis of how the p.Gln424Pro mutation affects the physiological function of DCDC2a, we performed *in silico* analysis of the structural landscape of DCDC2a (Fig. 1D; 5–7). Our analysis suggests that, with the exception of the first 250 residues, which harbor a tandem pair of structured doublecortin domains interrupted by an unstructured interdomain linker and flanked by unstructured terminal loops, the DCDC2a polypeptide chain adopts a predominantly unstructured tail spanning over 200 C-terminal residues. However, the DCDC2a tail harbors a canonical PXXPXR motif (residues 447–452) located within the vicinity of p.Gln424Pro mutation (Fig. 1C). The PXXPXR motif represents a consensus sequence for the binding of a wide array of SH3-containing proteins, which include many protein kinases that play central roles in cellular signaling and trafficking (8). Importantly, many of these SH3-containing proteins are involved in cytoskeletal organization. It is thus possible that the p.Gln424Pro mutation alters DCDC2a's ability to interact with cellular SH3-containing partners.

In early postnatal rat and mouse inner ears, we used immunopurified antibodies for which we characterized the specificity to DCDC2a by immunocytochemistry (Fig. 2A–E) and western blotting (Fig. 2F), and immunolocalized DCDC2a to the kinocilia of inner, outer and vestibular hair cells and to the primary cilia of all supporting cell types (Fig. 2G, H, K–M and O). Moreover, DCDC2a was found associated with the cellular microtubule network (Fig. 2N). Quantification of DCDC2a immunofluorescence along the length of the ampullar kinocilia showed localization along its entire length, with significantly increasing concentrations towards the tip (Fig. 2P).

In order to examine the targeting properties of DCDC2a, we performed biolistic transfections of plasmidic DNA constructs encoding for wild-type and p.Gln424Pro mutant DCDC2a-GFP in hair cells and supporting cells of early postnatal rat inner ear organotypic cultures, as well as in non-polarized COS7 cells (Fig. 3). In COS7 cells, both wild-type and p.Gln424Pro mutant DCDC2a-GFP disrupted the intracellular microtubule network by inducing the formation of extended cytosolic microtubule cables (Fig. 3A, C and D) (9), compared with GFP alone (Fig. 3B); cytoskeletal actin, however, did not appear to be affected (Fig. 3C and D). In hair cells and supporting cells, overexpression of wild-type or p.Gln424Pro mutant DCDC2a-GFP was found to cause elongation of kinocilia and primary cilia (Fig. 3F–S). Quantification of the effect of DCDC2a on cilia length showed that p.Gln424Pro mutant DCDC2a-GFP causes an average of a 2–3-fold increase in cilia length, compared with wild-type DCDC2a-GFP (Fig. 3T–V). Besides cilia length deregulation, supporting cells and hair cells expressing p.Gln424Pro mutant DCDC2a-GFP showed a diversity of cilia anomalies, such as branching along the primary cilia (Fig. 3P), duplication and triplication of primary cilia (Fig. 3Q–S) and stereocilia bundle degeneration (Fig. 3M). We were not able to reproduce these effects of wild-type and mutant DCDC2a-GFP expression on polarized Madin Darby Canine Kidney type II (MDCK-II) epithelial cell (data not shown) nor on non-polarized COS7 cell (Fig. 2B–E) primary cilia structure.

We studied *dcdc2b* morpholino-mediated knockdown in zebrafish. The survival of the larvae was very sensitive to the morpholino dose. Using a subminimal dose of morpholino (MO) targeting on the intron 4–exon 5 acceptor-splicing site (Fig. 4K, Supplementary Material, Table S1), we obtained living morphants that showed minimal whole body developmental deformations or delays, with no gross morphological changes to the otolithic organ. In these MO morphants, we detected by RT–PCR a higher fraction of mRNA intron 4 retention, a very small fraction of exon 5 skip, as well as a high amount of normal, mature mRNA (Fig. 4I). In contrast to the larvae injected with a control morpholino (CoMO) (Fig. 4) which showed normal body development and swimming behavior similar to wild-type non-injected larvae, MO morphants were not capable of swimming or hearing (Fig. 4). They also showed a high level of hair cell abnormalities, such as body deformations, and often the internalization of the stereocilia hair bundles and their respective kinocilia (Fig. 4G and H), despite, in cases, the presence of normal hair cell counts in the neuromasts (Fig. 4I and J); this reflects the early steps of hair cell degeneration. We also observed a high level of hair cell degeneration in both the lateral line neuromasts and the inner ear reflected by a much lower number of hair cells (Fig. 4C–F, M and N). Microphonic recordings from the otic vesicle showed a significant reduction of hair cell response to stimuli and higher microphonic threshold for MO morphants, which correlate with significant reduction in the number of saccular hair cells (Fig. 4O–Q). These results support our hypothesis that *dcdc2b* is essential for the general development of zebrafish larvae and for hair cell development and survival.

Discussion

Here, we discovered that the DCDC2a p.Gln424Pro mutation causes recessive isolated deafness in humans. DCDC2a belongs to a superfamily of doublecortin-like (DCX) domain containing proteins (10). DCX domains appear in the proteins encoded by the X-linked doublecortin (*DCX*) gene, mutations in which cause abnormal neuronal migration, epilepsy and mental retardation, the retinitis pigmentosa-1 gene (*RP1*), the three *DCDC2* genes (*DCDC2a*, *DCDC2b* and *DCDC2c*) and in six other gene products (10). DCX domains have conserved and unique roles in cytoskeletal structure regulation, microtubule-based transport and signal transduction (9). Doublecortin proteins bind microtubules and regulate complex microtubule-dependent processes that involve many interacting proteins. Moreover, intronic SNPs in *DCDC2a*—located in a *DYX2* locus that is associated with reading disability, language impairment and IQ on chromosome 6p22—were found to be associated with human dyslectic reading disabilities (11,12). Together with *KIAA0319*, *DCDC2a* is predicted to be a major effector gene in DYX2. Further characterization of the *DYX2* locus suggested *CMAHP* and *FAM65B* as DYX2 candidate effector genes (13). Comparisons between *Dcdc2a* knockout mice and wild-type littermates revealed no significant differences in neuronal migration, neocortical lamination, neuronal

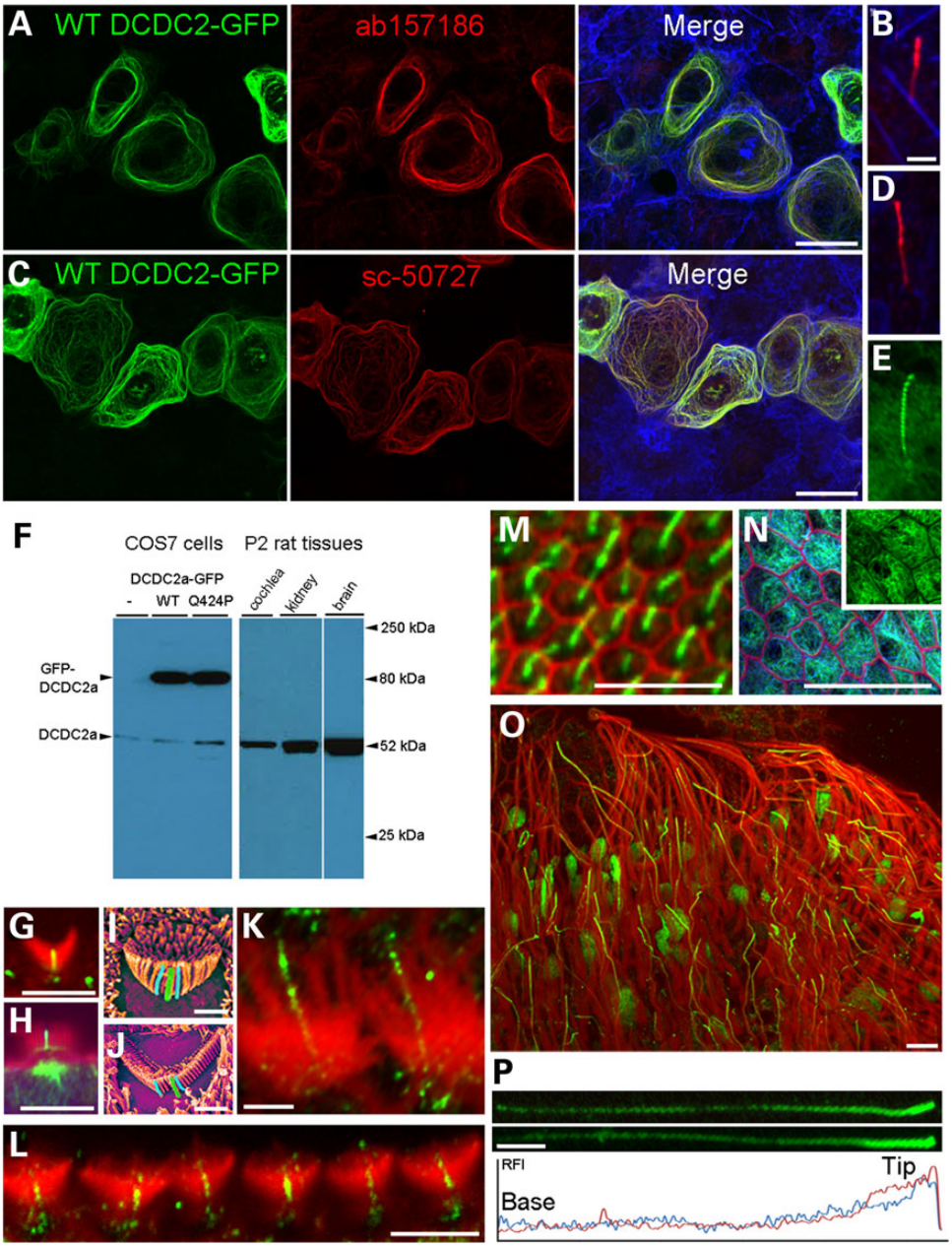

Figure 2. Antibody specificity validation and wholemount immunofluorescence on rat inner ear tissues. (**A–E**) DCDC2a rabbit monoclonal antibody ab157186 (red subpanel in A) and goat polyclonal antibody sc-50727 (red subpanel in C) validation by immunocytochemistry on COS7 cells expressing DCDC2a-GFP (green subpanels in A and C) showing colocalization (Merge subpanels in A and C); actin in blue. DCDC2a is endogenously expressed in COS7 cells and localizes to primary cilia, revealed through a surface confocal scan in non-transfected cells by both antibodies ab157186 (B) and sc-50727 (D). DCDC2a-GFP also targets primary cilia (E). Comparable cilia lengths were estimated to ~12 μm in COS7 cells expressing (E) or not (B and D) exogenous DCDC2a-GFP. (**F**) Left panel: western blots of protein extracts of COS7 cells expressing wild-type (WT) or p.Gln424Pro mutant (Q424P) DCDC2a-GFP and non-expressing controls (-) using ab157186 rabbit monoclonal antibody (Abcam; dilution: 1/2000) showing a faint band of ~52 kDa that reflects endogenous expression of DCDC2a, and an upper intense band of ~80 kDa corresponding to the recombinant DCDC2-GFP wild-type and mutant proteins. Right panel: western blot of protein extracts of select postnatal Day 2 (P2) rat tissues: cochlea sensory epithelia, kidney and brain using ab157186 antibody, showing a unique ~52 kDa band, corresponding to the predicted size of DCDC2a. (**G**, **H** and **K–P**) Wholemount immunofluorescence on P2 rat inner ear sensory epithelia using ab157186 rabbit monoclonal antibody (G, H, K and M–P) (Abcam, dilution: 1/700) and sc-50727 goat polyclonal antibody (L) (Santa Cruz, dilution: 1/200), showing the localization of DCDC2a (green) in kinocilia of outer (G and L), inner (H) and vestibular saccule (K) and ampulae (O) hair cells, as well as to the primary cilia of supporting cells (M) and associated to cytoskeletal microtubule network of hair cells (H) and supporting cells (N); actin in red; acetylated α-tubulin in blue in H and N. (I and J) Adobe photoshop-processed scanning electron micrographs of mouse P2 outer hair cells from the apex (H) and the mid-base (J) of the cochlea showing the chevron-shaped developing stereocilia bundle staircase formation (two of the tallest stereocilia in light blue) and the positioning of the kinocilium (green). Note that the kinocilium has a comparable size relative to that of the tallest stereocilia. (P) DCDC2a relative immunofluorescence intensity profile of two isolated ampullar kinocilia. Scale bars: 20 μm in A and C; 5 μm in B, D, E, G, H and K–P; 2 μm in I and J.

ciliogenesis or dendritic differentiation (14). These results suggest that *Dcdc2a* is not required for neurogenesis, neuronal migration or differentiation, but may have partial functional redundancy with *Dcx* (15). In *Drosophila*, however, a doublecortin-containing microtubule-associated protein DCX-EMAP has been localized to the tubular body in campaniform receptors

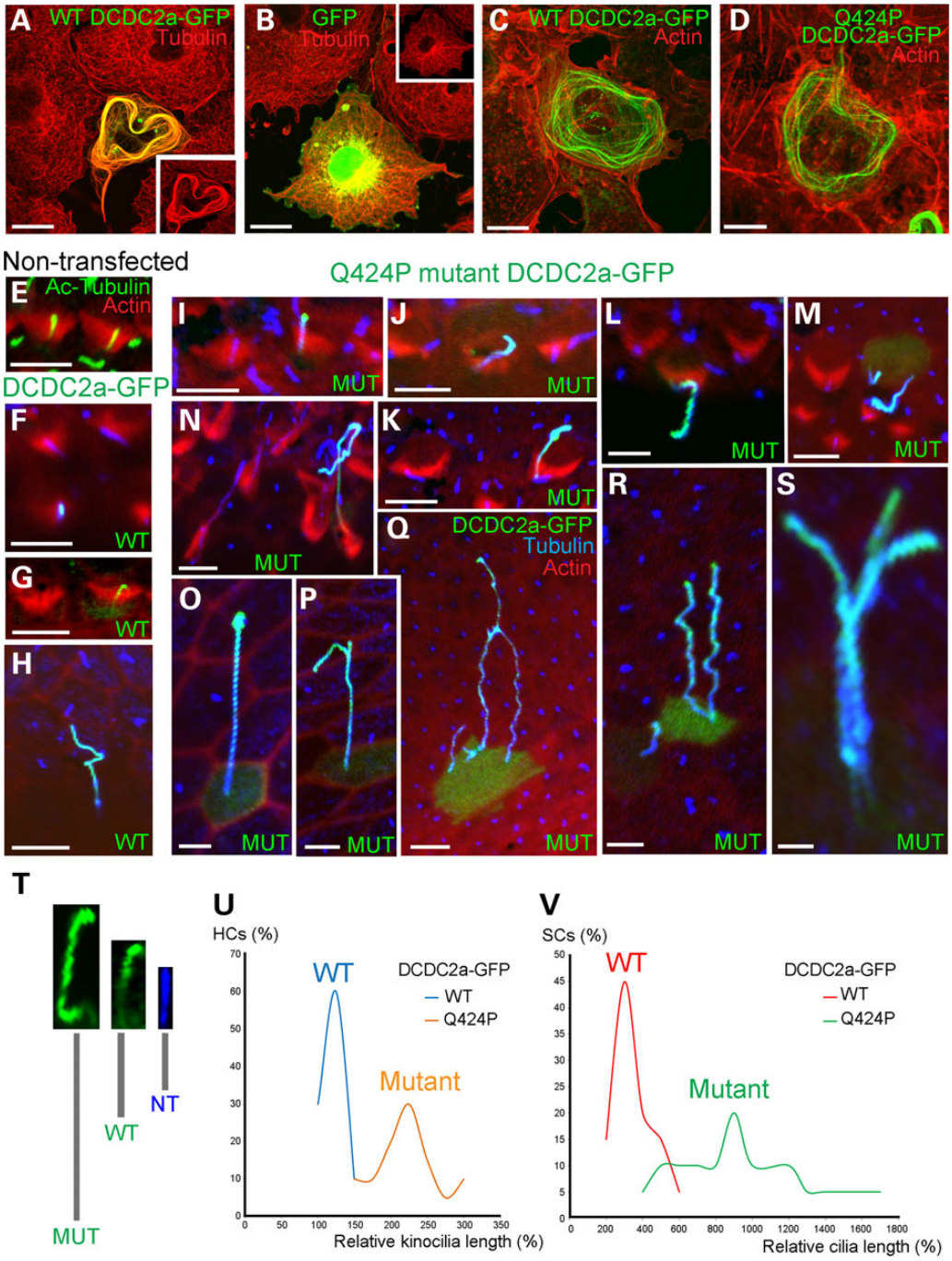

Figure 3. Cellular localization of wild-type and p.Gln424Pro mutant DCDC2-GFP in COS7 cells and rat inner ear sensory epithelium organotypic culture hair cells and supporting cells. (**A**, **C** and **D**) Expression of wild-type (A and C) and p.Gln424Pro mutant (D) DCDC2-GFP (green) in COS7 cells led to a change in microtubule network organization (red in A) and the formation of extended microtubule cables to which DCDC2-GFP localizes. (**B**) Expression of GFP alone does not change microtubule network (Red). Cytoskeletal actin network (red in C and D) is not affected. (**E**) Wholemount immunofluorescence of P2 rat organotypic mid-apical turn cochlea outer hair cell stereocilia hair bundle (actin in red) showing the location and the length of normal kinocilia (α-acetylated tubulin in green). (**F–H**) Representative confocal images of outer hair cells (F and G) and supporting cell (H) expressing wild-type DCDC2a-GFP (WT) showing its localization in kinocilia (F and G) and primary cilium (H), and caused a slight (G) or no (F) relative kinocilium elongation (~100–150%) and a more important extension of primary cilium (~600%); kinocilia and primary cilia are visualized in blue by immunostaining α-acetylated tubulin. (**I–L**) Representative confocal micrographs of organ of Corti outer hair cells showing an increasing effect of the mutant p.Gln424Pro DCDC2-GFP (MUT) on the kinocilium relative length ranging from ~150% (I) to ~300% (L). (**M**) A hair cell expressing p.Gln424Pro DCDC2-GFP with a duplication of the kinocilium and an absence of its stereocilia hair bundle. (**N**) A vestibular hair cell expressing mutant p.Gln424Pro DCDC2-GFP showing a remarkable elongation of the kinocilium compared with that of its neighbor hair cells. (**O–S**) Supporting cells expressing p.Gln424Pro DCDC2-GFP showing exaggerated cilia lengths compared with those of their respective neighbor cells, and also showing a variety of anomalies ranging from cilium branching (P), to cilium duplication or triplication (Q–S). (**T**) Same scale kinocilia confocal micrographs (green) of outer hair cells expressing p.Q424P mutant [MUT, (L)] and wild-type [WT, (G)] DCDC2-GFP, and that of non-transfected outer hair cells (blue) from the cochlea apical turn, as well as length bars (gray) showing their respective unfolded lengths. (**U** and **V**) Quantification of the relative length of outer hair cells kinocilia (U) and supporting cells cilia (V) in cells expressing wild-type DCDC2-GFP [blue in (U) and red in (V)] or mutant p.Gln424Pro DCDC2-GFP [orange in (U) and green in (V)]. Quantifications have been performed on 20 outer hair cells (HCs) and 20 supporting cells (SCs) expressing either wild-type (WT) or mutant (MUT) protein with average cilium elongation ratios = 123 ± 15% for HCs expressing WT, 223 ± 45% for HCs expressing MUT, 350 ± 110% for SCs expressing WT and 907 ± 322% for SCs expressing MUT. The differences in elongation ratios in HCs and SCs expressing WT and MUT DCDC2a were statistically significant with *P*-values <0.0001. Scale bars: 10 μm in (A–D), 5 μm in (E–R) and 2 μm in (S).

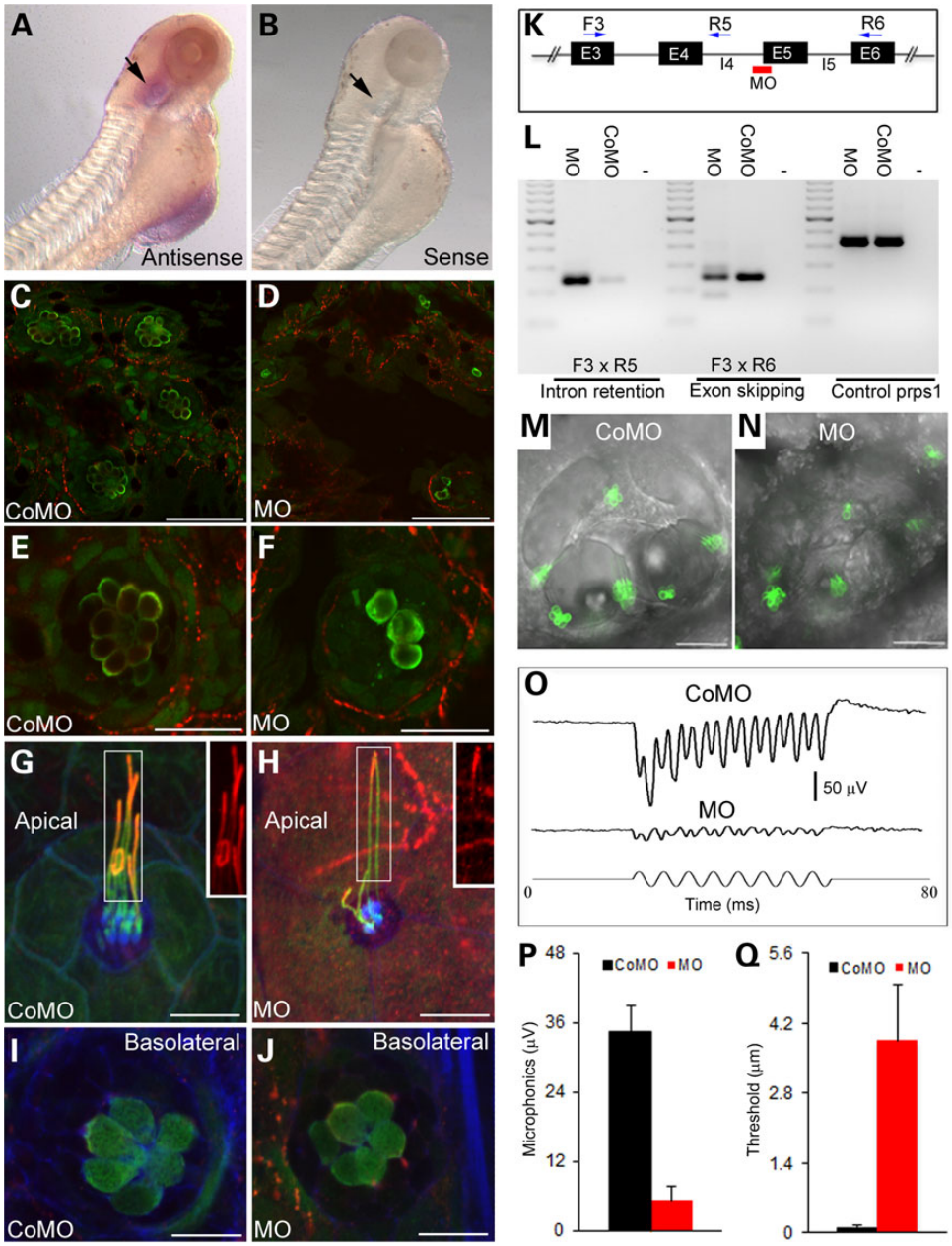

Figure 4. Zebrafish model for *dcdc2b*-related sensorineural hearing loss. (**A** and **B**) Whole-mount *in situ* hybridization of 3-day post-fertilization (dpf) zebrafish larvae with *dcdc2b* antisense (A) and sense (B) riboprobes. The arrow in (A) indicates *dcdc2b* expression in the otic vesicle, and the absence of signal in (B). (**C–J**) Whole-mount immunofluorescence on neuromast hair cells (GFP positive) of 3-dpf *Tg(pou4f3:gap43-GFP)* larvae injected with a control morpholino (CoMO; C, E, G and I) and on larvae injected with a *dcdc2b*-specific morpholino (MO; D, F, H, and J); GFP is in green, actin is counterstained in blue, and acetylated α-tubulin in red. Optical scans through hair cell bodies (expressing GFP in green) of CoMO fish show normal neuromast hair cells (C, E and I), while the majority of the MO fish have abnormal neuromasts with fewer hair cells (D and F). (G and I) Apical and basalolateral scans of a head neuromast from a CoMO fish showing a rosette pattern of six hair cell bodies (green in I) and their six corresponding stereocilia bundles (blue in G) and their six kinocilia (red in G). (H and J) Apical and basolateral scans of an equivalent head neuromast from a MO fish showing six hair cell bodies (green in J) with only four stereocilia bundles (blue in H) and four kinocilia (green in H). Kinocilia microtubule core anomalies in MO are also reflected by the abnormal α-acetylated tubulin immunofluorescence pattern (red in H, inset) compared with CoMO's (red in G, inset). (**K**) A schematic drawing of exons 3–6 of the zebrafish *dcdc2b* gene showing binding sites of a MO (red bar) and RT–PCR primers (blue arrows). (**L**) RT–PCR products from MO and CoMO zebrafish showing intron 4 retention and exon 5 skip in MO. (**M** and **N**) Confocal images of otic vesicles of live CoMO and MO *Tg(pou4f3:gap43-GFP)* fish at 3 dpf, showing reduction in number of crista hair cells in MO. (**O**) Microphonic potential waveforms of CoMO (upper trace) and MO fish (middle trace) in response to 200-Hz sinusoidal stimuli (lower trace) at 2.9-µm displacement. (**P**) Comparison of microphonic amplitude (root mean square) between CoMO ($n = 6$) and MO ($n = 8$) fish. Stimuli: 200 Hz at 2.9-µm displacement. (**Q**) Comparison of microphonic thresholds between CoMO ($n = 6$) and MO ($n = 6$) fish. Student's *t*-tests were performed to determine the significance of differences. Data presented in O, Q and **R** are means ± SEM, $P < 0.0001$. Scale bars: 50 µm in (C, D, M and N), 20 µm in (E and F), 10 µm in (G–J).

and to the ciliary dilation in chordotonal mechanoreceptors in Johnston's organ, the fly's auditory organ, and DCX-EMAP has been implicated in mechanotransduction in the fly's sensory cilia (15).

Using immunofluorescence, we also show that DCDC2a is a microtubule-associated protein that distributes uniformly along the sensory hair cell kinocilium but with a significantly increasing concentration towards its tip, that could be the result of an

active tip-directed transport. Moreover, we present evidence that p.Gln424Pro mutation deregulates kinocilia axoneme length and stability, as has been reported in hippocampal neuron culture primary cilia (16). Since microtubule-associated proteins (MAPs), such as doublecortin proteins, have been proposed to regulate kinesin cargo-transport (17), these observations suggest that p.Gln424Pro DCDC2a mutation might disrupt the transport of microtubule length-regulation cargos within the inner ear cilia. The absence of effects of DCDC2 exogenous expression on MDCK-II epithelial cell or on non-polarized COS7 cell primary cilia structure, would reflect molecular differences between inner ear epithelia, and kidney and primary cell lines ciliary cargo transport systems and their regulatory molecules.

The kinocilium is a specialized primary cilium nucleated from the hair cell centrioles, called the basal body that plays a role in hair bundle morphogenesis and the intrinsic polarity of individual hair cells (18). During development of mammalian sensory hair cells, soon after the hair cells exit the cell cycle, the kinocilium migrates from the center to the lateral edge of the hair cell apex, followed by the growth of surrounding microvilli which begin to assemble into a staircase to form a chevron-shaped hair bundle with the kinocilium located at the vertex of the chevron next to the tallest row of stereocilia. Cilia assembly and maintenance require a highly regulated intraflagellar transport (IFT) process during which particles are bidirectionally carried along axonemal microtubules (19–21). Disruption of IFT leads to human ciliopathies that affect ciliated tissues ranging from the eye, gut and brain to the kidney (22,23). It is well documented that the length of hair cell stereocilia is tightly regulated in order for them to constitute a mechanically excitable staircase formation (24–26). Scanning electron microscopy shows that within outer hair cells from the cochlea apex to basal turns, there are similarities in lengths of the tallest stereocilia and the kinocilium (Fig. 2I and J). Kinocilia are physically connected during hair bundle development via extracellular linkages formed between protocadherins PCDH15 and CDH23; these linkages are essential for proper hair bundle formation and the intrinsic polarity of individual hair cells that constitute a coordinated polarity among all hair cells known as planar cell polarity (PCP, 27). Thus, defects in kinocilia length regulation would be predicted to impact the development of the stereocilia hair bundle and its planar cell polarity.

Interestingly, in rat hippocampal neurons Dcdc2a was found to interact with kinesin motor Kif3a (16). Kif3a has proved to be crucial for hair cell kinocilia and supporting cell ciliogenesis, and for hair cell PCP (28). We speculate that kinocilium anomalies caused by DCDC2a p.Gln424Pro mutation would in turn alter the cohesion and polarity of the developing stereocilia hair bundle. DCDC2a is therefore the first deafness-causing protein described so far to be important for the length regulation of kinociliary microtubule core. Further studies will elucidate the mechanisms and molecular environment of kinociliary microtubule length-regulation system related to DCDC2a.

Materials and Methods

Subjects and clinical evaluations

This study was approved by institutional review boards (IRB) of the University of Miami, and by the Ethical Committee of the University Hospital of Mahdia, Tunisia. Written informed consent was obtained from adult subjects and the parents of minor subjects. Clinical history interviews and physical examinations of members of FT2 family ruled out environmental factors as causing the hearing loss and the presence of a syndrome. Later, these family members were contacted for further renal examination which showed no anomalies. The degree of hearing impairment was assessed by pure audiometry test that was performed to test air conduction and bone conduction at frequencies ranging from 250 to 4000 Hz. Peripheral blood samples were collected from participant subjects for genomic DNA extraction following a standard phenol–chloroform method.

Whole exome sequencing

Genomic DNA from one affected individual in the family underwent whole exome sequencing. The SureSelect Human All Exon 50 Mb kit (Agilent, Santa Clara, CA, USA) was used for in-solution enrichment of coding exons and flanking intronic sequences following the manufacturer's standard protocol. Adapter sequences for the Illumina Hiseq2000 were ligated and the enriched DNA samples were subjected to standard sample preparation for the Hiseq2000 instrument (Illumina, San Diego, CA, USA). Paired-end reads of 99 bases length were produced. The Illumina CASAVA v1.8 pipeline was used to produce 99 bp sequence reads. Burrows-Wheeler Aligner (BWA) was used to align sequence reads to the human reference genome (hg19) and variants were called using the Genome Analysis Toolkit (GATK) software package. All variants were submitted to SeattleSeq134 for further characterization.

We filtered the variants using the Genomes Management Application (GEMapp), University of Miami Miller School of Medicine (https://secureforms.med.miami.edu/hihg/gem-app) according to the inheritance mode (homozygous autosomal recessive), to the function class including missense, nonsense, splice sites, in-frame indels and frame-shift indels, presence and frequency at the dbSNP137 and NHLBI (http://evs.gs.washington.edu/EVS/) databases (minor allele frequency of <0.5% was used). We also filtered the variants for their absence in more than two families in our internal database that includes over 2000 exomes. GATK quality score (QUAL) was set to 100 and genotype quality (GQ) was set to 75.

Mutation analysis by Sanger sequencing on genomic DNA

Exon 10 of the DCDC2a gene has been amplified (primers sequence in Supplementary Material, Table S1) in all sampled members of FT2 family and control individuals, and Sanger-sequenced on ABI models 3700 and 3100 automated sequencer (Applied Biosystems). Sequence data were aligned and compared with DCDC2a mRNA reference sequence NM_001195610. Mutation position was assigned referring to mRNA reference sequence NM_001195610.1 with nucleotide 1 as the first of the ATG start codon. The *DCDC2a* mutation has been assigned an identity number SCV000188610 in ClinVar database (http://www.ncbi.nlm.nih.gov/clinvar/).

Genbank accession numbers

Human DCDC2a protein: NP_001182539.1; Human *DCDC2a* mRNA: NM_001195610.1, zebrafish *dcdc2b* mRNA: NM_001037689.1.

Constructs encoding for DCDC2a and immunocytochemistry

Plasmid construct (catalog number: RG208721) encoding for C-terminally GFP-tagged human DCDC2a variant 1 under the control of CMV promoter (in pCMV6-AC-GFP vector) has been

purchased from OriGene. To introduce p.Gln424Pro substitution into DCDC2a expression plasmidic construct, we used site-directed mutagenesis kit (Stratagene). Clones obtained were fully sequenced and correct mutated clones were isolated and plasmid DNA preparations were made. Immunocytochemistry was performed on COS7 cells expressing the wild-type of the p.Gln424Pro mutant DCDC2-GFP as described (29).

Animal use

Sprague–Dawley rat 4-week-old adults and P2 pups, mouse P1–2 pups, wild-type AB, *Et(krt4:GFP)*^{sqet4} and *Tg(pou4f3:gap43-GFP)* zebrafish were used in this study. All procedures were approved by the University of Miami Institutional Animal Care and Use Committee following the National Institutes of Health guidelines on 'Using Animals in Intramural Research (http://oacu.od.nih.gov/training/PI/main_menu.htm)'.

Scanning electron microscopy

Freshly dissected cochleae of P1–2 mouse pup cochleae were processed for scanning electron microscopy by OTOTO (osmium-thiocarbohydrazide-osmium-thiocarbohydrazide-osmium) method as described (29) and viewed on a Hitachi S-4800 (Hitachi) operating at 5 kV.

Antibody validation and whole mount immunofluorescence preparations

Ab157186 DCDC2a rabbit monoclonal antibody was purchased from Abcam. Sc-50727 DCDC2a goat polyclonal antibody was obtained from Santa Cruz. Both antibodies were tested for specificity by immunocytochemistry on COS7 cells expressing DCDC2a-GFP and western blot of proteins from several P2 rat tissues and from COS7 cells expressing DCDC2a-GFP, as described (29). Ab157186 showed high specificity on western blot (dilution: 1/2000) and in immunocytochemistry on COS7 cells (dilution: 1/700). Sc-50727 did not reveal bands on western blot but showed high specificity by immunocytochemistry and similar DCDC2a localization pattern as ab157186 in immunofluorescence on wholemount inner ear preparations (dilution 1/50). Wholemount immunofluorescence preparations on postnatal Day 2–3 rat pup and on adult rats were performed as described (29). Images were taken on a LSM710 confocal microscope equipped with a ×63 1.4 numerical aperture (N.A.) objective (Zeiss Microimaging). Confocal images were processed using Adobe photoshop and NIH ImageJ was used for fluorescence quantifications.

Helios gene gun transfections

P2–3 organotypic rat hair cells and supporting cells were transfected with constructs encoding either wild-type DCDC2a-GFP or p.Glu424Pro mutant DCDC2a-GFP as described (29). It is important to mention that the gold particles used for gene gun transfections for both constructs were coated in the exact same conditions and using identical ratios of plasmid construct amount versus gold particles weight = 30 μg of plasmidic DNA/20 mg of 1 μm-diameter gold particles. Explants were fixed and processed for wholemount immunofluorescence exactly 24 h after gene gun transfection, and were counterstained with either rhodamin or Alexafluor-647 fluorescently-tagged phalloidin for actin, and with monoclonal acetylated α-tubulin (catalog # 32-2700; Invitrogen) reveled with a donkey anti-mouse Alexafluor-647 secondary (Invitrogen). The lengths of kinocilia of hair cells expressing or not expressing DCDC2a-GFP from the same high magnification confocal micrograph of organ of Corti preparations that were counterstained for α-acetylated tubulin to visualize kinocilia have been measured using NIH ImageJ software. The relative kinocilium length has been calculated as a ratio between the kinocilium length of hair cell expressing DCDC2a-GFP, and kinocilium length of neighbor non-transfected hair cell. Similar estimations have been performed on the effect of expression of either wild-type or mutant DCDC2a-GFP expressed in either hair cells or in supporting cells.

Zebrafish *dcdc2b in situ* hybridization, morpholino knockdown, RT–PCR, immunofluorescence, saccular hair cell quantification and hearing assessment

The expression of *dcdc2b* has been tested by *in situ* hybridization on 3-day post-fertilization (dpf) zebrafish larvae (wild-type AB), as described (30). Two sets of Digoxigenin-labeled RNA sense and antisense probes were *in vitro* synthesized using T3 and T7 RNA polymerases (Promega), respectively, on a PCR amplicon template obtained on a zebrafish randomly reverse-transcribed mRNA from zebrafish (*Danio rario*), using primers that were flanked by T3 and T7 RNA polymerase promoter sequences (Supplementary Material, Table S1). At least 10 larvae were used for each probe.

To generate zebrafish larvae with reduced *dcdc2b* function, we designed a splice-blocking morpholino, MO (Supplementary Material, Table S1, GeneTools) targeting the junction between intron 4 and exon 5. Embryos at the one-cell stage were injected with either MO (0.125–0.25 mM, 2 nl) or a control morpholino (Supplementary Material, Table S1, GeneTools) with the same dose. The efficiency of *dcdc2b* knockdown was assessed by RT–PCR of morpholino-induced exon 5 skip and intron 4 retention using the primers: F3 × R6 and F3 × R5, respectively (Supplementary Material, Table S1), as described (4). *Prps1* was amplified as a positive control. For phenotypic assessment, MO morphants were compared with stage-matched control zebrafish injected with CoMO.

Wholemount immunofluorescence on 3 dpf CoMOs and MO *Tg(pou4f3:gap43-GFP)* fish expressing GFP in hair cells were performed after fixing the fish in 3% PFA for 1 h. Larvae were permeabilized with 0.5% Triton-X100 for 30 min under gentle horizontal rocking, then blocked with 5% BSA in ×1 PBS for 1 h, then rabbit polyclonal GFP antibody (dilution 1/300; Abcam; catalog # ab290) and monoclonal acetylated α-tubulin antibody (dilution 1/100; Invitrogen; catalog # 32-2700) were applied for 2 h. The specimens were then washed three times with ×1 PBS, and anti-rabbit Alexafluor-488 together with anti-mouse Alexafluor-568 secondary antibodies and phalloidin Alexafluor-647 were added and incubated for 1 h. The specimens were finally washed three times with 1× PBS and mounted with Antifade mounting medium (Molecular Probes). Images were taken on LSM710 confocal microscope (Zeiss microimaging).

For visualization of hair cells in the inner ear, transgenic *Tg(pou4f3:gap43-GFP)* zebrafish with GFP expression in the cytoplasma membrane of hair cells were examined at 3 dpf. Zebrafish larvae were laterally embedded in 1.8% agarose and then scanned using a Nikon C1 confocal microscope to visualize live hair cells in three cristae of the inner ear. The number of crista hair cells in CoMO *Tg(pou4f3:gap43-GFP)* was compared with that of MO *Tg(pou4f3:gap43-GFP)*.

To assess auditory function of larval zebrafish, microphonic potentials were recorded from hair cells in the otic vesicle of 3-dpf zebrafish in response to a vibrating stimulus probe driven by a piezoelectric actuator (30). The stimulus probe was

positioned against the posterior end of the otic vesicle to provide the sinusoidal displacement at 200 Hz. The recording electrode was a beveled glass micropipette filled with fish saline.

Supplementary Material

Supplementary Material is available at *HMG* online.

Acknowledgements

We gratefully thank all the subjects in this study for their collaboration. We thank Dr Uri Manor (National Institutes of Health) for his critical reading and input on the manuscript.

Conflict of Interest statement. None declared.

Funding

This study was supported by the National Institutes of Health grants R01DC005575, R01DC012115 and R01DC012546 to X.Z.L., R01GM083897 and the Sylvester Comprehensive Cancer Center to A.F., R21DC009879, the University of Miami Provost Research Award and the College of Arts and Sciences Gabelli Fellowship to Z.L. This work was also supported by funds from the ICGEB (International Centre for Genetic Engineering and Biotechnology) and the Ministry of Higher Education and Research of Tunisia to S.M.

References

1. Michalski, N. and Petit, C. (2014) Genetics of auditory mechano-electrical transduction. *Pflugers Arch. Eur. J. Physiol.*, **467**, 49–72.
2. Tlili, A., Männikkö, M., Charfedine, I., Lahmar, I., Benzina, Z., Ben Amor, M., Driss, N., Ala-Kokko, L., Drira, M., Masmoudi, S. and Ayadi, H. (2005) A novel autosomal recessive non-syndromic deafness locus, DFNB66, maps to chromosome 6p21.2–22.3 in a large Tunisian consanguineous family. *Hum. Hered.*, **60**, 123–128.
3. Bensaïd, M., Hmani-Aifa, M., Hammami, B., Tlili, A., Hakim, B., Charfeddine, I., Ayadi, H., Ghorbel, A., Castillo, I.D. and Masmoudi, S. (2011) DFNB66 and DFNB67 loci are non allelic and rarely contribute to autosomal recessive nonsyndromic hearing loss. *Eur. J. Med. Genet.*, **54**, e565–e569.
4. Diaz-Horta, O., Subasioglu-Uzak, A., Grati, M., DeSmidt, A., Foster, J. II, Cao, L., Bademci, G., Tokgoz-Yilmaz, S., Duman, D., Cengiz, F.B. *et al.* (2014) FAM65B is a membrane-associated protein of hair cell stereocilia required for hearing. *Proc. Natl Acad. Sci. USA*, **111**, 9864–9868.
5. Dosztanyi, Z., Csizmok, V., Tompa, P. and Simon, I. (2005) IUPred: web server for the prediction of intrinsically unstructured regions of proteins based on estimated energy content. *Bioinformatics*, **21**, 3433–3434.
6. Ishida, T. and Kinoshita, K. (2007) PrDOS: prediction of disordered protein regions from amino acid sequence. *Nucleic Acids Res.*, **35**, W460–W464.
7. Shimizu, K., Hirose, S. and Noguchi, T. (2007) POODLE-S: web application for predicting protein disorder by using physicochemical features and reduced amino acid set of a position-specific scoring matrix. *Bioinformatics*, **23**, 2337–2338.
8. Sparks, A.B., Hoffman, N.G., McConnell, S.J., Fowlkes, D.M. and Kay, B.K. (1996) Cloning of ligand targets: systematic isolation of SH3 domain-containing proteins. *Nat. Biotechnol.*, **14**, 741–744.
9. Coquelle, F.M., Levy, T., Bergmann, S., Wolf, S.G., Bar-El, D., Sapir, T., Brody, Y., Orr, I., Barkai, N., Eichele, G. and Reiner, O. (2006) Common and divergent roles for members of the mouse DCX superfamily. *Cell Cycle*, **5**, 976–983.
10. Dijkmans, T.F., van Hooijdonk, L.W., Fitzsimons, C.P. and Vreugdenhil, E. (2010) The doublecortin gene family and disorders of neuronal structure. *Cent. Nerv. Syst. Agents Med. Chem.*, **10**, 32–46.
11. Meng, H., Smith, S.D., Hager, K., Held, M., Liu, J., Olson, R.K., Pennington, B.F., DeFries, J.C., Gelernter, J., O'Reilly-Pol, T. *et al.* (2005) DCDC2 is associated with reading disability and modulates neuronal development in the brain. *Proc. Natl Acad. Sci. USA*, **102**, 17053–17058.
12. Powers, N.R., Eicher, J.D., Butter, F., Kong, Y., Miller, L.L., Ring, S.M., Mann, M. and Gruen, J.R. (2013) Alleles of a polymorphic ETV6 binding site in DCDC2 confer risk of reading and language impairment. *Am. J. Hum. Genet.*, **93**, 19–28.
13. Eicher, J.D., Powers, N.R., Miller, L.L., Mueller, K.L., Mascheretti, S., Marino, C., Willcutt, E.G., DeFries, J.C., Olson, R.K., Smith, S.D. *et al.* (2014) Characterization of the DYX2 locus on chromosome 6p22 with reading disability, language impairment, and IQ. *Hum. Genet.*, **133**, 869–881.
14. Wang, Y., Yin, X., Rosen, G., Gabel, L., Guadiana, S.M., Sarkisian, M.R., Galaburda, A.M. and Loturco, J.J. (2011) Dcdc2 knockout mice display exacerbated developmental disruptions following knockdown of doublecortin. *Neurosci.*, **190**, 398–408.
15. Bechstedt, S., Albert, J.T., Kreil, D.P., Müller-Reichert, T., Göpfert, M.C. and Howard, J. (2010) A doublecortin containing microtubule-associated protein is implicated in mechanotransduction in Drosophila sensory cilia. *Nat. Commun.*, **1**, 11.
16. Massinen, S., Hokkanen, M.E., Matsson, H., Tammimies, K., Tapia-Páez, I., Dahlström-Heuser, V., Kuja-Panula, J., Burghoorn, J., Jeppsson, K.E., Swoboda, P. *et al.* (2011) Increased expression of the dyslexia candidate gene DCDC2 affects length and signaling of primary cilia in neurons. *PLoS One*, **6**, e20580.
17. Atherton, J., Houdusse, A. and Moores, C. (2013) MAPping out distribution routes for kinesin couriers. *Biol. Cell*, **105**, 465–487.
18. Tilney, L.G., Tilney, M.S. and DeRosier, D.J. (1992) Actin filaments, stereocilia, and hair cells: how cells count and measure. *Annu. Rev. Cell Biol.*, **8**, 257–274.
19. Goetz, S.C. and Anderson, K.V. (2010) The primary cilium: a signalling centre during vertebrate development. *Nat. Rev. Genet.*, **11**, 331–344.
20. Nigg, E.A. and Raff, J.W. (2009) Centrioles, centrosomes, and cilia in health and disease. *Cell*, **139**, 663–678.
21. Jones, C., Roper, V.C., Foucher, I., Qian, D., Banizs, B., Petit, C., Yoder, B.K. and Chen, P. (2008) Ciliary proteins link basal body polarization to planar cell polarity regulation. *Nat. Genet.*, **40**, 69–77.
22. Waters, A.M. and Beales, P.L. (2011) Ciliopathies: an expanding disease spectrum. *Pediatr. Nephrol.*, **26**, 1039–1056.
23. Davis, E.E. and Katsanis, N. (2012) The ciliopathies: a transitional model into systems biology of human genetic disease. *Curr. Opin. Genet. Dev.*, **22**, 290–303.
24. Belyantseva, I.A., Boger, E.T., Naz, S., Frolenkov, G.I., Sellers, J.R., Ahmed, Z.M., Griffith, A.J. and Friedman, T.B. (2005) Myosin-XVa is required for tip localization of whirlin and differential elongation of hair-cell stereocilia. *Nat. Cell Biol.*, **7**, 148–156.
25. Peng, A.W., Belyantseva, I.A., Hsu, P.D., Friedman, T.B. and Heller, S. (2009) Twinfilin 2 regulates actin filament lengths in cochlear stereocilia. *J. Neurosci.*, **29**, 15083–15088.

26. Manor, U., Disanza, A., Grati, M., Andrade, L., Lin, H., Di Fiore, P.P., Scita, G. and Kachar, B. (2011) Regulation of stereocilia length by myosin XVa and whirlin depends on the actin-regulatory protein Eps8. *Curr. Biol.*, **21**, 167–172.
27. Webb, S.W., Grillet, N., Andrade, L.R., Xiong, W., Swarthout, L., Della Santina, C.C., Kachar, B. and Müller, U. (2011) Regulation of PCDH15 function in mechanosensory hair cells by alternative splicing of the cytoplasmic domain. *Development*, **138**, 1607–1617.
28. Sipe, C.W. and Lu, X. (2011) Kif3a regulates planar polarization of auditory hair cells through both ciliary and non-ciliary mechanisms. *Development*, **138**, 3441–3449.
29. Grati, M. and Kachar, B. (2011) Myosin VIIa and sans localization at stereocilia upper tip-link density implicates these Usher syndrome proteins in mechanotransduction. *Proc. Natl Acad. Sci. USA*, **108**, 11476–11481.
30. Lu, Z. and DeSmidt, A.A. (2013) Early development of hearing in zebrafish. *J. Assoc. Res. Otolaryngol.*, **14**, 509–521.